

https://doi.org/10.1070/QEL17329

Investigation of the effect of noise parameters of a 3D lidar on the error in estimating relief signatures of distant objects from 2D field intensity distributions of reflected radiation

V.I. Ivanov, N.I. Ivanov

Abstract. **We consider the influence of noise parameters of a 3D lidar and external background radiation on the error in estimating the relief signatures of distant objects from 2D field intensity distributions of the reflected radiation. A physical and mathematical model is developed to analyse the effect of noise. The dependence of the error in estimating the relief signatures at various signal-to-noise ratios is investigated taking into account the parameters of real multi-element photodetectors (MEPDs). The obtained results indicate the possibility of evaluating relief signatures of distant objects with high accuracy based on standard MEPDs simultaneously for a large number of points on the object's surface with a signal-to-noise ratio of more than 4.**

Keywords: *3D lidar, 3D images, 3D cameras.*

1. Introduction

Increasing the efficiency of detection and recognition of various dynamically changing objects, including low-contrast and zero-contrast objects, is the main task in the development and fabrication of modern laser ranging systems, including imaging and automated recognition systems [1–5]. The priority direction for solving this task is the development of 3D non-scanning lidars (3D Flash LIDAR), which ensure the acquisition of relief characteristics of objects simultaneously on a set of elements with dimension $N = n_x \times n_y$ on their surface in the form of a 2D map of depths ξ_{ij} (distances R_{ij}) of each n_{ij}th surface element [4–6]. In lidars of these types, reflected signals are photodetected and processed by specialised 3D cameras (3D LIDAR imaging cameras), which are highly integrated solid-state systems based on multi-element photodetectors (MEPDs), namely, single-photon avalanche photodiode (SPAD) arrays [6, 7] and multichannel processors. These processors contain tens of thousands of time-measuring 'start-stop' channels and measure time intervals between the moment of laser pulse emission, t_0, and the moments of reflected signal arrival, t_{ij}, at each n_{ij}th element of the MEPD. The solution of this problem on the basis of algorithms for temporal 'start-stop' measurements using hybrid technologies by combining many separate time-measuring channels (see, for example, [8]) significantly limits the ability to determine the relief characteristics of objects with a high spatial resolution, since with an increase in the dimension N of the relief depth map, the same number of elementary photodetectors and parallel operating time-measuring channels are required.

An alternative to time-of-flight methods for obtaining relief signatures of distant objects, which does not require specialised processors with N time-measuring channels, is the laser 3D location method relying on the energy ratios of partial beams in 2D energy distributions of the reflected field [9]. The basic concept of the method was first proposed by us in patents [10, 11], and the method itself was first used in [12, 13]. In this work, we study the influence of noise parameters of a lidar and external background on an error in estimating relief signatures of distant objects and examine the features of practical implementation of the modified algorithm of this method based on a MEPD with charge accumulation.

2. Concept of the method

In accordance with the algorithm of the method in question [9], the surface of an object located at a distance R from the lidar is irradiated with laser pulses havng an increased beam divergence. The duration of laser pulses is determined from the relation

$$\tau_{\rm p} > \frac{2\xi_{k\max}(\boldsymbol{r})}{c}, \tag{1}$$

where $\xi_{k\max}(\boldsymbol{r})$ is the maximum relief depth at the kth point of the object surface; $\boldsymbol{r}$ is the vector with coordinates x and y in the object plane; and c is the speed of light.

In the complex of recognition problems, automated recognition of remote small-size objects is of great practical importance [1, 8]. The class of such objects includes small-size aircraft; ground, surface and underwater vehicles; armoured vehicles; sea mines; unexploded ordnance; fragments of wrecked objects; parameters of sea waves for detecting underwater explosions and moving underwater objects by their surface manifestations; etc. The maximum relief depth of objects of this class does not exceed 3–4.5 m, which, in accordance with (1), determines the minimum laser pulse duration equal to $\tau_{\rm p} \approx 20–30$ ns.

A reflected signal $E_k(\boldsymbol{r}, t)$ arriving at a MEPD input with dimension N can be represented as a set of fields of N partial beams (sub-beams) of laser radiation. A partial beam is understood as reflected laser radiation incident on a photocell (pixel) of a MEPD located in the image plane of the receiving optical system (OS). The dimension N of the MEPD is determined by the required spatial resolution of the lidar in the object plane.

V.I. Ivanov, N.I. Ivanov Institute for Nuclear Problems, Belarusian State University, ul. Bobruiskaya 11, 220030 Minsk, Belarus; e-mail: ivanov.inp@gmail.com

Received 18 March 2020; revision received 30 March 2020
Kvantovaya Elektronika **50** (11) 1068–1073 (2020)
Translated by I.A. Ulitkin

The distribution of the time delay (shift) $\tau_k(\boldsymbol{S})$ of each subbeam of the reflected radiation is uniquely related to the distribution of the relief depth $\xi_k(\boldsymbol{r})$ of the object surface by the expression

$$\tau_k(\boldsymbol{S}) = 2\xi_k(\boldsymbol{r})/c, \tag{2}$$

where $\boldsymbol{S}$ is the vector with coordinates x and y in the plane of the MEPD, which can be a matrix photodetector with charge accumulation, for example, a CCD array.

The maximum value of the delay time of the partial beam of the reflected signal is determined by the expression

$$\tau_{k\max}(\boldsymbol{S}) = 2\xi_{k\max}(\boldsymbol{r})/c. \tag{3}$$

The instant t_1 of arrival of the leading edge of the reflected pulse relative to the instant t_0 of laser pulse emission τ_p is

$$t_1 - t_0 = 2R_b/c, \tag{4}$$

where R_b is the base distance to the surface point with a maximum elevation corresponding to $\xi_k = 0$.

For an object with a diffusely scattering surface, the field amplitude in the image plane of the receiving OS is determined as the sum of the fields reflected from individual points of the surface in the OS direction:

$$E(\boldsymbol{S}) = \sum_k E_{0k}(\boldsymbol{r},t)\,K(\boldsymbol{r},t)\,T_a(\boldsymbol{S},t)\,A_k(\boldsymbol{S}) = \sum_k E_k(\boldsymbol{S}), \tag{5}$$

where $E_{0k}(\boldsymbol{r},t)$ is the distribution of the complex amplitude of the laser radiation field on the surface; $K(\boldsymbol{r},t)$ is the distribution of the surface reflection coefficient; $T_a(\boldsymbol{S},t)$ is the transfer function of the medium through which the laser radiation is transferred along the location path (atmosphere, hydrosphere); $A_k(\boldsymbol{S})$ is the instrument transfer function of the lidar OS; and $E_k(\boldsymbol{S})$ is the field amplitude in the image of the kth point of the surface.

In the general case, the propagation of laser radiation in an inhomogeneous atmosphere results in fluctuations in the propagation time of laser radiation along the location path and an increase in the duration of laser pulses. These phenomena are mainly caused by fluctuations in the angles of laser radiation propagation in an inhomogeneous atmosphere due to fluctuations in the refractive index of the atmosphere along the location path. The influence of refraction and atmospheric turbulence on the propagation of laser signals has been investigated in many works, for example, in [14–21]. As shown in [16–19], the largest fluctuations in the angles of arrival of laser radiation (up to 5′) are caused by the effects of anomalous refraction. The frequency of such fluctuations is 10^{-3}–10^{-2} Hz. The significantly higher frequency of fluctuations in the angles of arrival (up to 10^3 Hz) is associated with thermal turbulence in the atmosphere. However, the amplitude of such fluctuations is much less than the refractive fluctuations and does not exceed 5″ [20]. The low-frequency nature of these processes determines the time of the quasi-stationary state of the atmosphere, which is tens of thousands of times longer than the propagation time and exposure time of signals at each location cycle.

According to [15, 21], the root-mean-square fluctuations in the propagation time and duration of laser pulses when they pass along atmospheric paths are insignificant. For example, when laser pulses propagate along a horizontal atmospheric path with medium turbulence (structural refractive index $C_n^2(h) = 10^{-14}$–5×10^{-14} м$^{-2/3}$) at a distance of 10–15 km, these time fluctuations are within 0.68–1 ps. For inclined and vertical paths, they can be even smaller: When propagating along vertical paths through the entire thickness of the atmosphere, the root-mean-square fluctuations in the propagation time of the laser signal and the pulse duration are no more than 0.07 ps, and when propagating at an angle of 80°, no more than 0.17 ps [21]. This gives reason to believe that the pulse duration for each partial beam of reflected radiation is equal with a high degree of accuracy to the duration of the emitted laser pulse τ_p, and the propagation time of the laser pulse along a path of a given length is constant.

Three-dimensional distributions of the depth $\xi_k(\boldsymbol{r})$ of the object's surface relief are determined from the ratio of the energies of partial beams for two 2D distributions $B_1(\boldsymbol{S})$ and $B_2(\boldsymbol{S})$ of the reflected light field energy:

$$\theta(\boldsymbol{S}) = B_1(\boldsymbol{S})/B_2(\boldsymbol{S}). \tag{6}$$

Distributions $B_1(\boldsymbol{S})$ and $B_2(\boldsymbol{S})$ are obtained at different exposure (accumulation) times. The distribution $B_1(\boldsymbol{S})$ is found by accumulating the energy $E(\boldsymbol{S},t)$ of the reflected light field in a spatiotemporal gate of duration $\tau_{s1} = \tau_p$ in the interval $(t_1, t_1 + \tau_p)$, which includes the leading edge of the pulse, or in the interval $(t_1 + \tau_p, t_1 + 2\tau_p)$ for the trailing edge of the pulse. Consequently, the distribution $B_1(\boldsymbol{S})$ for the realisation section $E(\boldsymbol{S},t)$ containing the leading edge of the pulse is determined by the expression

$$B_1(\boldsymbol{S}) = |E_k(\boldsymbol{S})|^2 \int_{t_1}^{\tau_p} f^2(t-\tau_k)\,dt = |E_k(\boldsymbol{S})|^2(\tau_p - \tau_k), \tag{7}$$

where

$$f^2(t-\tau_k) = \begin{cases} 1 \text{ for } t = \tau_k, \\ 0 \text{ for } t \neq \tau_k. \end{cases}$$

The $B_2(\boldsymbol{S})$ distribution is obtained by accumulating the field energy $E(\boldsymbol{S},t)$ in a gate of duration SiO_2, equal to the duration $T = \tau_p + \tau_{k\max}$ of the reflected signal. Therefore, the distribution $B_2(\boldsymbol{S})$ can be written as

$$B_2(\boldsymbol{S}) = |E_k(\boldsymbol{S})|^2 \int_{t_1}^{t_1+T} f^2(t-\tau_k)\,dt = |E_k(\boldsymbol{S})|^2\tau_p. \tag{8}$$

In accordance with (7) and (8), expression (6) takes the form

$$\theta(\boldsymbol{S}) = \frac{\tau_p - \tau_k(\boldsymbol{S})}{\tau_p}. \tag{9}$$

From (9) we find the 2D distribution of the delay time of the partial beams of the reflected radiation $\tau_k(\boldsymbol{S})$ with respect to the time instant t_1, and, consequently, to t_0:

$$\tau_k(\boldsymbol{S}) = \tau_{s1} - \tau_p\frac{B_1(\boldsymbol{S})}{B_2(\boldsymbol{S})} = \tau_{s1} - \tau_p\theta(\boldsymbol{S}) = \tau_p - \tau_p\theta(\boldsymbol{S}). \tag{10}$$

From (10), taking into account relation (2), we determine the relief signature of the object under study:

$$\xi_k(\boldsymbol{r}) = \frac{c}{2}[\tau_p - \tau_p\theta(\boldsymbol{S})], \tag{11}$$

and also a map of the distances $R_{\xi_k}(\boldsymbol{r})$ to the points of the surface relief:

$$R_{\xi_k}(\boldsymbol{r}) = R_\mathrm{b} + \xi_k(\boldsymbol{r}). \quad (12)$$

The basic distance R_b is measured by a time-measuring 'start-stop' lidar channel with threshold detection of the moment of the reflected signal arrival t_1, along which gating pulses with durations τ_{s1} and τ_{s2} are also formed.

3. Model for analysing the influence of noise parameters

A mixture of a reflected laser signal and background radiation of the atmosphere and sky enters the input of a MEPD lidar. Taking into account background radiation and equations (7) and (8), the ratio θ'_{ij} for a partial beam with coordinates x_i and y_j in the $\theta(\boldsymbol{S})$ distribution can be written in the form:

$$\theta'_{ij}(\tau_k) = \frac{B_{1ij}}{B_{2ij}} = \frac{(P_{sij} + P_\mathrm{b})(\tau_\mathrm{p} - \tau_k) + P_\mathrm{b}\tau_k}{(P_{sij} + P_\mathrm{b})\tau_\mathrm{p} + P_\mathrm{b}\tau_\mathrm{p}} = \frac{P_{sij}(\tau_\mathrm{p} - \tau_k) + P_\mathrm{b}\tau_\mathrm{p}}{(P_{sij} + 2P_\mathrm{b})\tau_\mathrm{p}}, \quad (13)$$

where P_{sij} and P_b are the powers of the partial beam of the reflected signal and background radiation that are incident on a MEPD photocell, respectively; and subscripts i and j define the coordinates x_i and y_j of the photocell n_{ij} in the MEPD field.

Taking into account the fact that $W_\mathrm{s} = P_\mathrm{s}\tau_\mathrm{p}$ and $W_\mathrm{b} = P_\mathrm{b}\tau_\mathrm{p}$ are the energies of the reflected signal and background incident on a MEPD photocell, and that the factor $P_\mathrm{s}(\tau_\mathrm{p} - \tau_k) = W_\mathrm{s}(1 - m_k)$, where $m_k = \tau_k/\tau_\mathrm{p}$ is the information parameter of the relief depth ξ_k, equation (13) for the number of photons N_s and N_b has the form

$$\theta'_{ij}(\tau_k) = \frac{[W_\mathrm{s}(1 - m_k) + W_\mathrm{b}]/W_\mathrm{ph}}{(W_\mathrm{s} + 2W_\mathrm{b})/W_\mathrm{ph}} = \frac{N_\mathrm{s}(1 - m_k) + N_\mathrm{b}}{N_\mathrm{s} + 2N_\mathrm{b}}, \quad (14)$$

where $W_\mathrm{ph} = h\nu$ is the photon energy of probe radiation.

Providing short-term exposures of 2D fields in specified temporal gates of short duration $\tau_{s1(s2)}$ is possible both with the use of external high-speed modulators (shutters) (see, for example, [22, 23]) installed in front of the MEPD, and by direct electronic control of the process of photoelectric conversion and amplification in the MEPD-CCDs themselves, as well as in hybrid electron-optical converters (HEOCs), which are electron-optical converters (EOCs) whose fluorescent screen is coupled to the CCD [24, 25].

The high speed and low level of control electrical signals (no more than 5 V) of selective GaAs-based electro-absorption modulators [22, 23] make their application promising. However, the strong temperature dependence of the centre wavelength of the pass-band requires temperature stabilisation of modulators of these types or the use of lasers with a similar temperature dependence of the generated radiation wavelength. Low-voltage gating (electronic shutter) is also easily implemented in a CCD: for a CCD with avalanche photodiodes, $\tau_\mathrm{s} \geqslant 0.2$ ns [26]; for a CCD, $\tau_\mathrm{s} \geqslant 40$ ns [27]. For HEOCs, $\tau_\mathrm{s} \geqslant 0.4$ ns [25], but high-voltage control pulses are required.

Despite the disadvantages inherent in all HEOCs based on EOCs with a fluorescent screen, which consist in increasing noise and decreasing the dynamic range with an increase in the gain of the EOC, the use of HEOCs allows one to provide high sensitivity of a 3D lidar and 'fast' signal gating. Construction of photodetector channels (PDCs) of a lidar based on new developments of HEOCs with direct electronic excitation of a CCD placed inside the vacuum volume of an EOC [28] makes it possible to eliminate the above disadvantages and provide record sensitivity indicators.

The operation of photoelectric conversion of signals (13), taking into account the influence of noise and external background radiation in a PDC based on a HEOC, can be described by the equation

$$\theta'_{ij}(\tau_k) = \left\{K_1[N_\mathrm{s}(1 - m_k) + N_\mathrm{b}] + \sqrt{K_1\mu_{s1}[N_\mathrm{s}(1 - m_k) + N_\mathrm{b}] + \bar{N}^2_\mathrm{qd} + \bar{N}^2_\mathrm{qr} + \bar{N}^2_\mathrm{qQv}}\right\} \times \left[K_2(N_\mathrm{s} + 2N_\mathrm{b}) + \sqrt{K_2\mu_{s2}(N_\mathrm{s} + 2N_\mathrm{b}) + \bar{N}^2_\mathrm{qd} + \bar{N}^2_\mathrm{qr} + \bar{N}^2_\mathrm{qQv}}\right]^{-1} K_\mathrm{c}^{-1}, \quad (15)$$

where K_1 and K_2 are the coefficients of the photoelectric conversion of the energy of the input light signal incident on a single photocell of the PDC into an electrical output signal: for a HEOC

$$K_{1(2)} = \eta_1 G K' \eta_2, \quad (16)$$

for a CCD without internal amplification

$$K_{1(2)} = \eta_2 K'; \quad (17)$$

where η_1 and η_2 are the quantum efficiencies of the EOC and the CCD, respectively; G is the gain; K' is the loss factor of the receiving and matching optics; $\mu_{s1(s2)}$ is the noise factor proportional to the gain G of the light signal in the PDC and introducing additional noise during photoelectron conversion with gain $G \gg 1$ (for example, at $G \approx 10^5 - 10^6$, $\mu_{s1(s2)} = 1.2 - 3.5$ [29, 30]); and $\bar{N}^2_\mathrm{qd}$, $\bar{N}^2_\mathrm{qr}$ and $\bar{N}^2_\mathrm{qQv}$ are the squares of the average values of the CCD noise components: the number of dark current electrons, the number of readout electrons, and the number of analogue-to-digital conversion (ADC) noise electrons of the CCD charges (quantisation noise), respectively.

The real difference in the photoelectric conversion coefficients for each PDC pixel ($K_1 \neq K_2$) for the correct interpretation of the measurement results requires knowledge of their ratio K_{1ij}/K_{2ij}, which is reflected in equation (15) by the calibration factor

$$K_{cij} = K_{1ij}/K_{2ij}. \quad (18)$$

The coefficients K_{cij} are determined experimentally by measuring the ratios of the energies $\theta'_{cij} = K_{cij}$ for the distributions $B_1(\boldsymbol{S})$ and $B_2(\boldsymbol{S})$ according to (15) under uniform illumination of the PDC in the linear region of its sensitivity by radiation from a uniformly illuminated screen and are recorded in the memory of the lidar calculator.

Estimates of the influence of the signal-to-noise ratio $\psi_1$on the error in determining the relief characteristics require taking into account the noise parameters of the PDC and the power of background radiation. The effect of these parameters is especially significant for the $B_1(\boldsymbol{S})$ distribution. This is due to the fact that, in contrast to the $B_2(\boldsymbol{S})$ signal, the actual energy accumulation time of the $B_1(\boldsymbol{S})$ signal decreases with increasing m_k, i. e., with increasing relief depth, which leads to

a proportional decrease in the signal energy $N_s(1 - m_k)$, and, consequently, to the deterioration of the signal-to-noise ratio that, in accordance with (14) for B_1, is determined by the expression

$$\psi_1 = \frac{K_1[N_s(1 - m_k) + N_b]}{\sqrt{K_1\mu_{s1}[N_s(1 - m_k) + N_b] + \bar{N}_{qd}^2 + \bar{N}_{qr}^2 + \bar{N}_{qQv}^2}}. \quad (19)$$

As follows from (19), the ratio ψ_1 reaches its minimum value at $m_{k\max}$, which corresponds to the maximum relief depth $\xi_{k\max}$. The factor $(1 - m_{k\max})$ in (19) can be expressed as

$$1 - m_{k\max} = (\tau_p - \tau_{k\max})/\tau_p = \frac{\Delta\tau_{\min}}{\tau_p}, \quad (20)$$

where $\Delta\tau_{\min}$ determines the required resolution in terms of relief depth:

$$\Delta\xi = \frac{c}{2}\Delta\tau_{\min}. \quad (21)$$

The resolution $\Delta\xi$ is understood as the ability to measure a certain minimum change in the depth of the relief with a given error, which accordingly determines the number of distinguishable gradations of relief depths in a given range.

Taking into account (20), expression (19) can be written in the form

$$\psi_1 = \frac{K_1\left[N_s\left(\frac{\Delta\tau_{\min}}{\tau_p}\right) + N_b\right]}{\sqrt{K_1\mu_{s1}\left[N_s\left(\frac{\Delta\tau_{\min}}{\tau_p}\right) + N_b\right] + \bar{N}_n^2}}, \quad (22)$$

where $\bar{N}_n^2 = \bar{N}_{qd}^2 + \bar{N}_{qr}^2 + \bar{N}_{qQv}^2$.

Equation (22) determines the minimum value of the ratio ψ_1 for a given $\Delta\tau_{\min}$. An increase in the resolution (a decrease in $\Delta\xi = f(\Delta\tau_{\min})$) is unambiguously associated with an increase in ψ_1, which is due to the choice of a photodetector with a low noise index $\bar{N}_n^2$ and an increase in energy $N_s(\Delta\tau_{\min}/\tau_p)$.

4. Influence of noise parameters on the estimation error of the relief signature of an object

We estimate the effect of PDC noise for a HEOC-based lidar containing an EOC with a fluorescent screen and a Kodac KAI-1003M CCD image sensor [31]. This matrix is characterised by a relatively low threshold sensitivity (40 electrons without taking into account the noise introduced by the ADC of the CCD charges). At the same time, it has a large potential well depth (charge packet capacity) of a pixel, $N_{q\max} = 170000$ electrons, which is important both for measurements at a large signal-to-noise ratio and for expanding the dynamic range in assessing the relief depth. The estimates are carried out for a laser pulse duration $\tau_p = 30$ ns.

Numerical estimates of the noise components $\bar{N}_{qd}$, $\bar{N}_{qr}$ and $\bar{N}_{qQv}$ *for the Kodac KAI-1003M CCD image sensor*. The number of dark current electrons $\bar{N}_{qd}$ is defined as the noise charge of the dark current i_d in time τ:

$$\bar{N}_{qd} = i_d\frac{\tau}{qG} = n_q\tau, \quad (23)$$

where q is the electron charge, and n_q is the average number of dark current electrons.

According to the technical data sheet of the sensor [31], the electron count rate of the dark current, reduced to the area of one pixel, is 2500 electrons per second. Accordingly, the number of dark current electrons during an accumulation time of 30 ns will not exceed 7.5×10^{-5}.

Readout noise of the CCD pixel charge is $\bar{N}_{qr} = 40$ electrons [31]. The need to obtain relief signatures in digital form introduces an additional error due to quantisation noise. The root-mean-square value of the quantisation noise is determined according to [32] from the expression

$$\bar{N}_{qQv}^2 = \Delta_{Qv}^2/12, \quad (24)$$

where $\Delta_{Qv} = N_{q\max}/2^n$ is the quantisation step, which is set by the ADC capacity of 2^n. For the CCD potential well depth, $N_{q\max} = 170000$ electrons and for a 10-bit ADC ($2^{10} = 1024$), $\bar{N}_{qQv}^2 = 166^2/12 = 2296$.

In accordance with the obtained estimates of the noise components, as applied to the problem of measuring the relief signature of objects with a relief depth of up to $\sim$4.5 m, the noise index $\bar{N}_n^2$ in (22) is 3896. Taking this into account, the signal-to-noise ratio, for example, at $\Delta\xi = 2$ cm, reaches units at the charge number N_{sq} of signal electrons of the CCD pixel equal to 63 (at $\mu_{s1} = 1.2$ for $G \approx 500 - 1000$), which corresponds to the number of photons of the partial beam of the reflected signal at the CCD input $N_{ss} = N_{sq}/\eta_2 = 210$, where $\eta_2 = 0.3$ is the quantum efficiency of the KAI-1003M CCD [31].

Numerical estimates of the power of external background radiation, expressed as the number of photons N_b during an exposure time of 30 ns, for background radiation of various nature are given in Table 1 according to [32].

The error in estimating the relief depth, which is determined by formula (11), can be represented in the form

$$\sigma_{\xi_{kij}} = \frac{c}{2}\sqrt{\sigma_{\tau_p}^2 + \sigma_{\theta_{kij}}^2}, \quad (25)$$

where $\sigma_{\tau_p}^2$ is the standard deviation of duration $\tau_{s1} = \tau_p$, caused by an error in measuring the duration of the laser pulse and fluctuations in the 'timing' of the gating pulse τ_p to the moment of arrival of the reflected signal t_1; and $\sigma_{\theta_{kij}}^2 = (\theta_{kij} -$

Table 1. Numerical estimates of the power of external background radiation.

Source of background radiation	Power P_b in the spectral range of laser radiation/W	Number of background radiation photons N_b
Scattered radiation from stars in a clear night atmosphere	8.7×10^{-21}	8.2×10^{-10}
Scattered solar radiation in a clear daytime atmosphere	8.7×10^{-14}	8.2×10^{-3}
Solar radiation reflected from clouds	3.5×10^{-13}	3.32×10^{-2}
Solar radiation reflected from the underlying surface	8.7×10^{-13}	8.2×10^{-2}

$\bar{\theta}'_{kij})^2$ is the standard deviation of the index $\bar{\theta}'_{kij}$, calculated by formula (15) with allowance for the given ratio ψ_1 (22), from the exact value θ_{kij} determined by formula (9).

Figure 1 shows the calculated dependences of σ_ξ on the relief depth of the object surface ξ for various signal-to-noise ratios. The analysis of these dependences testifies to the high accuracy of the method under consideration. The error in estimating the relief depth can be less than 2 cm. The 'pedestal' of the error $\sigma_\xi = f(\xi)$ on these dependences, equal to ~2 cm, is a systematic error introduced by the parameter σ_{τ_p} in (25), the value of which is ~0.14 ns and is mainly due to temporal fluctuations in the 'binding' of the beginning of measurements to the time of arrival of the reflected signal t_1 and the error in determining the laser pulse duration. The error in estimating the relief depth decreases with an increase in the signal-to-noise ratio ψ_1 and can be reduced by a factor of $\sqrt{n_z}$ when averaging the measurement results over a number of location cycles n_z. This statement is in good agreement with our experimentally averaged error value over several location cycles of test samples of a stepped relief, which was ~0.7 cm [9].

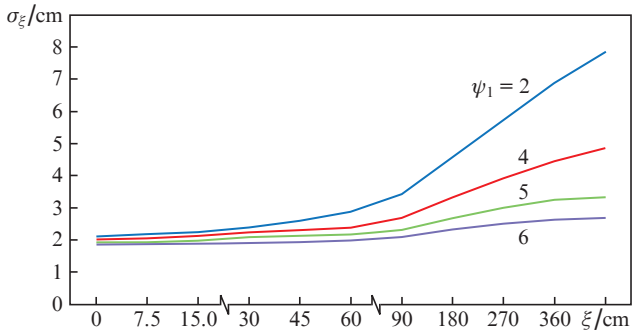

Figure 1. Dependences of the error σ_ξ on the relief depth of an object's surface ξ for different values of ψ_1.

The accuracy characteristics of the method fully satisfy the problem of remote detection and recognition of various objects [1, 33]. According to studies carried out in the United States [27], for the automated recognition of such objects by their relief signatures, the minimum information involves the discrete dimension of the field in the image plane of the object of $N = 200$ elements at a resolution in relief depth of ~15 cm, which is successfully achieved using the considered method even at relatively low signal-to-noise ratios.

5. Conclusions

The developed model for assessing the influence of the noise parameters of a 3D lidar makes it possible to numerically estimate the error in determining the relief signatures of distant objects, taking into account the noise parameters of real photodetectors and the background environment. The results obtained indicate the possibility of evaluating the relief signatures of objects with high accuracy on the basis of standard MEPDs simultaneously for a large number of points on the object surface with a signal-to-noise ratio $\psi_1 > 4$. Due to the short accumulation times of signals, the effect of natural background radiation on the estimation error of relief signatures is insignificant. The number of points on the object's surface can be tens and hundreds of thousands, depending on the required spatial resolution in the image plane of the object and is limited only by diffraction phenomena at the receiving aperture of the optical system and the available lidar pulse energy.

References

1. Wood J.J., Randall P.N., Nicholas M.R., Nothard J.M., Watson G.H., Harvey C., Smith G. *Proc. NATO Military Sensing Symposium* (Orlando, USA, 2008) p.147.
2. Baloev V.N., Mishanin S.S., Ovsyannikov V.A., Fillipov V.L., Yakubson S.E., Yatsyk V.S. *Opt. Zh.*, **79** (3), 22 (2017).
3. Belov V.V., Abramochkin V.N., Gridnev Yu.V., Kudryavtsev A.N., Kozlov V.S., Rakhimov R.F., Shmargunov V.P., Tarasenkov M.V. *Opt. Atmos. Okeana*, **30** (4), 285 (2017).
4. Itzler M. *Proc. ILMF 2015* (Denver, 2015) p.1.
5. Chua S.Y., Wang X., Guo N., Tan C.S., Chai T.Y., Seet G.L. *J. Eur. Opt. Soc.-Rapid*, **11**, 16015 (2016).
6. Carrara L., Fiergolski A. *Appl. Sci.*, **9**, 2206 (2019).
7. Giudici A., Simmerle D., Veronese D., Biasi R., Gulinatti A., Rech I., Ghioni M., Maccagnani P. *Fotonika*, **6** (36), 32 (2012).
8. Gryaznov N.A., Kuprenyuk V.I., Sosnov E.N. *Opt. Zh.*, **82** (2), 27 (2015).
9. Ivanov V.I., Ivanov N.I. *Quantum Electron.*, **48** (7), 679 (2018) [*Kvantovaya Elektron.*, **48** (7), 679 (2018)].
10. Ivanov V.I. Patent SU 1593429 A1, G01 S17/00. Priority date 4 January 1988.
11. Ivanov V.I. Patent SU 1591621 A1, G01 C3/08. Priority date 11 April 1988.
12. Ivanov V.I., *in Metody i sredstva distantsionnogo zondirovaniya Zemli i obrabotki kosmicheskoi informatsii v interesakh narodnogo khozyaystva* (Methods and means of remote sensing of the Earth and processing of space information in the interests of the national economy) (Ryazan, 1989) Pt. 1, p. 39.
13. Ivanov V.I., *in Vysokoskorostnaya fotografiya, fotonika i metrologiya bystroprotekayushchikh protsessov* (High-speed photography, photonics and metrology of fast processes) (Moscow, 1989) p. 114.
14. Tatarski V.I. *Wave Propagation in a Turbulent Medium* (New York: McGraw-Hill, 1961; Moscow: Nauka, 1967).
15. Zuev V.E., Banakh V.A., Pokasov V.V. *Optika turbulentmoi atmosfery* (Optics of a Turbulent Atmosphere) (Leningrad: Gidrometeoizdat, 1988) Vol. 5.
16. Kushtin I.F. *Refraktsiya svetovykh luchei v atmosfere* (Refraction of Light Rays in the Atmosphere) (Moscow: Nedra, 1974).
17. Lukin V.P. *Atmospheric Adaptive Optics* (Bellingham, Wash.: *SPIE*, 1995; Novosibirsk: Nauka, 1986).
18. Melamud A.E., Lukin V.P. Patent SU 1553828 A1, G01 C15/00. Priority date 26 June 1985.
19. Lukin V.P., Melamud A.E., Mironov V.L. *Izv. Vyssh. Uchebn. Zaved., Ser. Fiz.*, dep. VINITI No. 6774 (1984).
20. Prilepin M.T., Golubev A.N. *Opticheskie kvantovye generatory v geodezicheskikh izmereniyakh* (*Optical Quantum Generators in Geodetic Measurements*) (Moscow: Nedra, 1972).
21. Brookner E. *IEEE Trans. Commun. Techol.*, **4**, 396 (1970).
22. Sang Hun Lee, Chang Young Park, Yang-Woo You, Heesun Yoon, Yong-Chul Cho, Yong-Hwa Park. *Sensors and Actuators A: Physical*, **197** (1), 47 (2013).
23. Byung Hoon Na, Gun Wu Ju, Chang Young Park, Soo Kyung Lee, Hee Ju Choi, Yong Chul Cho, Yong Hwa Park, Yong Tak Lee. *Opt. Lett.*, **40** (14), 3376 (2015).
24. Medvedev A., Sokolov D.S. *Fotonika*, **6** (36), 42 (2012).
25. Morozova E.E., Podvyaznikov V.A., Sladkova E.S., Chevokin V.K. *Prib. Tekh. Eksp.*, **5**, 157 (2017).
26. Pancheri L., Dalla Betta G.-F., Stoppa D. *SPIE Newsroom*, 1 (2014). DOI:10.1117/2.1201405.005477.
27. Umbitaliev A.A., Tsykulin A.K., Mantsvetov A.A., Kozlov V.V., Rychazhnikov A.E., Baranov P.S., Ivanov A.V. *Opt. Zh.*, **79** (11), 84 (2012).
28. Alymov O.V., Levko G.V., Chukavina Yu.G., Chulkov V.G. *Izv. Yuzhogo Federal'nogo Univer., Ser. Tekh. Nauki*, **9** (122), 161 (2011).

29. Soboleva N.A., Melamid A.E. *Fotoelektronnye pribory* (Photoelectronic Devices) (Moscow: Vysshaya Shkola, 1974).
30. Edwards S. *Elektronnye Komponenty*, **11**, 19 (2013).
31. https://www.onsemi.com/pub/Collateral/KAI-1003-D.PDF.
32. Garnov S.V., Moiseeva A.V., Nosatenko P.Ya., Fomin V.N., Tserevitinov A.B. *Trudy IOFAN*, **70**, 26 (2014).
33. Zheng Q., Der S. *IEEE Trans. Image Proces.*, **10** (4), 897 (2001).